The Journal of Adhesion, 79: 749–776, 2003

ISSN: 0021-8464 print/1545-5823 online
DOI: 10.1080/00218460390214857

Taylor & Francis
Taylor & Francis Group

CONTACT BETWEEN A SMOOTH MICROSPHERE AND AN ANISOTROPIC ROUGH SURFACE

W. Cheng
P. F. Dunn
R. M. Brach
Particle Dynamics Laboratory,
Department of Aerospace and Mechanical Engineering,
University of Notre Dame, Notre Dame, IN, USA

This article discusses the effects of asperities on elastic and adhesive contact between a smooth sphere and a rough surface. Two numerical methods are introduced: an asperity-superposition method and a direct-simulation method. In the first method, geometric parameters such as asperity heights, orientations, and radii of curvature are identified by a least-squares regression of neighboring surface heights measured using an atomic force microscope. The rough surface is reconstructed by the superposition of these asperities. The modeling of adhesive and elastic contacts begins with the modeling of a single parabolic-shaped asperity contact. A generalized JKR model for an arbitrary parabola is developed to suit this purpose. The contact between the rough surface (represented by the supposition of parabolic-shaped asperities) and the sphere consequently is modeled by the mapping and integration of individual asperity contacts. In the second method, pure-elastic contact is modeled by half-space elastic theory. A contact-search algorithm is used to find solutions on the displacement and the contact-pressure distribution that satisfy both the load-displacement equation and the contact boundary conditions. Results from both methods are compared to reveal the effects of asperities on adhesion and elastic-contact pressure.

Keywords: Asperity; Surface roughness; Adhesion; Adhesive contact; Elastic contact; Generalized JKR model

Received 19 November 2002; in final form 3 April 2003.

The research described in this article was supported in its early stage by the Center for Indoor Air Research (Contract No. 96-06), the Electric Power Research Institute (Contract No. RP 8034-03) and, in its final stage, by Philip Morris Incorporated.

Address correspondence to Raymond M. Brach, 105 Hessert Center, University of Notre Dame, Notre Dame, IN 46556 USA. E-mail: raymond.m.brach.1@nd.edu

INTRODUCTION

Contact between rough surfaces has been studied for decades. Most contact models have been based on the superposition of contacts made by surface asperities. Earlier models assumed perfect elasticity, spherical shape, and a constant radius of curvature for the asperities [1, 2]. Asperity height distributions were assumed to be exponential or Gaussian [3]. Improved numerical techniques enabled asperity ellipticity and plasticity to be considered [4]. Yet, most models still are based on the linear superposition of asperity contacts. More realistic adhesion modeling can be done by including the overlapping of contact regions and the shape of the asperities. These topics are addressed in this paper.

The modeling of adhesive contact between rough surfaces is more difficult because of variations in the heights and sizes of asperities and interaction between asperities. Fuller and Tabor [3] studied the effects of roughness on adhesion by experiments and numerical analysis based on the JKR theory. In their study, asperities were assumed to be hemispheres with the same radii and the heights were modeled by a Gaussian distribution. Asperity adhesion was modeled according to the spherical-contact JKR theory. The overall contact force between the sphere and the rough surface then was estimated to be the integral sum of the forces exerted by all the spherical asperities whose height exceeded a given approach distance. The overlapping of contact regions of neighboring asperities was not taken into account.

In a previous study, Cheng *et al.* [5] studied the effects of submicrometer-to-nanometer scale roughness on adhesion by assuming that surface roughness is random and homogeneous. One aim of this article is to show the importance that the anisotropy of asperities and overlapping of contact regions have in contact modeling with larger roughness scales. Two methods used to find solutions of the displacement and pressure during contact are presented in this article: an asperity-superposition method and a direct-simulation method.

The first method is comprised of three steps: the modeling of the rough surface as a superposition of asperities, the contact modeling of a single asperity, and the modeling of the contact between the sphere and the rough surface, which is treated as a superposition of asperities. The asperities are assumed to be parabolas. Geometric parameters of the asperities, such as the locations and heights of the asperity peaks, orientations, and radii of curvature are identified by a least-squares regression of neighboring surface heights. These heights were determined from atomic force microscope (AFM) scans of the rough surface. The rough surface then is reconstructed by the

integration of these detected parabolas. The extracted geometry parameters also are used to calculate the statistical properties of the asperities, such as the distribution of asperity heights, the orientation of the radii of curvature, and a nondimensional number that describes the shapes of the asperities. The modeling of the adhesive and elastic contacts begins with the modeling of single parabolic-shaped asperity contact. A generalized JKR model for arbitrary parabolas is developed to suit this purpose. The contact between the rough surface (represented by the supposition of parabolic-shaped asperities) and the sphere then is modeled by the integration of individual asperity contacts.

The second method is based on the half-space approximation. To simplify the analysis, it is assumed that the sphere and the rough surface are frictionless. Therefore, the normal displacement of the sphere and the rough surface is determined solely by the normal load [9]. The surface of the contact bodies (the sphere and the rough surface) is divided into uniform rectangular meshes with a constant pressure distribution over each element. The contact pressure and displacement distribution then can be discretized into two-dimensional arrays. The continuous load-displacement equation from the half-space approximation becomes a system of linear equations. A simple and effective algorithm developed by Kalker [6, 7] is used to find the solutions for the contact pressure and displacement distribution that satisfy both the load-displacement relationship and the boundary conditions. Results from both methods are compared to show the effects that asperities have on adhesion and the elastic-contact pressure.

The overlapping of contact regions depends on two factors: the level of the normal and the tangential displacements and the initial spacing of the asperities over the contact area. This study discusses the situation of normal contact. For this case, the overlapping of contact regions depends upon the externally applied normal force (either tension or compression) and the location of the center of the sphere during contact. Simulation results show that when an external load is low, the deformation of individual asperities over the rough surface is local and overlapping between contact spots does not occur. Consequently, when the sphere is pulled off, individual contact spots do not overlap. Therefore, the method of the contact superposition of asperities can be used to estimate the pull-off force in rough surface contacts. Simulation also shows that the contact force not only is related to overall displacement but also to contact area location on the rough surface. The density, spacing, heights, and shapes of the asperities change over the rough surface. Variations in the statistical distribution of the contact force at the center of the sphere with changes over the rough surface are analyzed by both methods.

ASPERITY-SUPERPOSITION MODEL

The Generalized JKR Model for Parabolas

In the first method (the asperity-superposition method), the contact between the sphere and the rough surface is modeled as the integration of contacts of individual asperities. The modeling of the contact of a single asperity provides a foundation for the integration. The traditional JKR model is valid for the contacts between spheres. A generalized JKR model is developed in this section to describe the adhesive contact of a parabola, which is a more appropriate shape of an asperity's contact region.

As contact is made, a contact region around a single asperity is formed. Surface stresses are generated over the contact region to support the external load. In the current model, the contact forces are assumed to act only within the contact region. The contact area for a parabola and a surface is elliptic. Elastic half-space theory applies because of the small scale of the parabola and the small scale of the displacement. The contact pressure is assumed to be [9]:

$$p(x,y) = p_0\left[1 - \left(\frac{x}{a}\right)^2 - \left(\frac{y}{b}\right)^2\right]^{1/2} + p_1\left[1 - \left(\frac{x}{a}\right)^2 - \left(\frac{y}{b}\right)^2\right]^{-1/2}, \quad (1)$$

which acts over the elliptic subcontact region, $\Omega = \{(x,y)|\frac{x^2}{a^2} + \frac{y^2}{b^2} \leq 1\}$. Here x and y are the Cartesian coordinates with the origin located at the center of the ellipse and a and b represent the longer (major) and shorter (minor) radii of the ellipse, respectively, as shown in Figure 1. The pressure outside the contact area is assumed to be zero. The first term on the right side of Equation (1) is the Hertzian contact force derived from the Hertzian theory. The second term represents an adhesion force that produces a uniform deflection over the contact area. In the absence of adhesion, $p_1 = 0$ because no tensile stress can be sustained by the contact area. With the appearance of adhesion, $p_1 < 0$. Tensile stresses are formed when the magnitude of adhesion is larger than that of the Hertzian contact pressure. The integration of adhesion over the contact area is finite. However, at the periphery of the contact area, a singularity occurs because the tensile stress is unbounded. Some researchers consider this a limitation of JKR theory. The magnitude of the displacement within the elliptical contact region can be described by:

$$U(x,y) = \delta - Ax^2 - By^2. \quad (2)$$

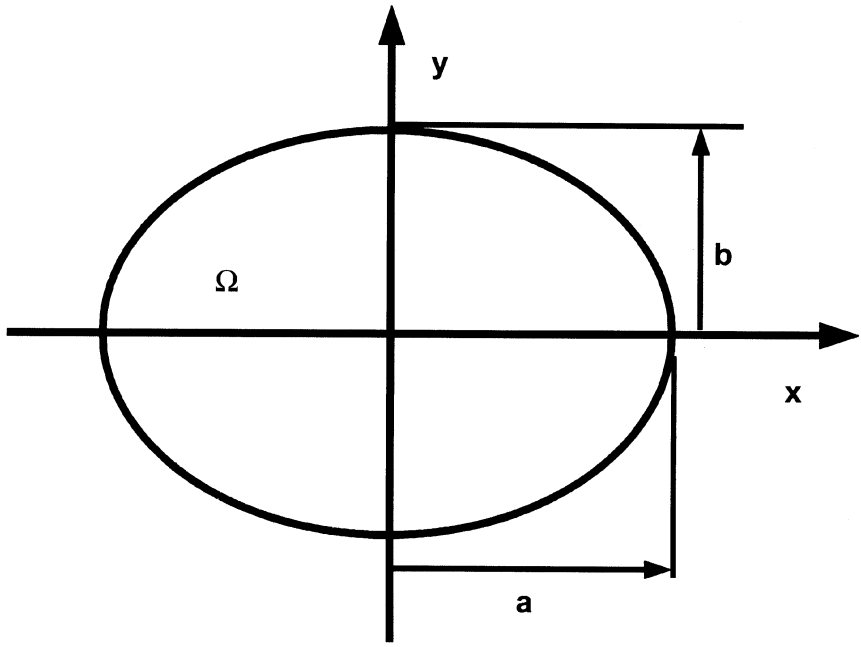

FIGURE 1 The schematic of the contact area of a single asperity.

According to the half-space elastic theory:

$$A = (p_0/E^*)(b/e^2a^2)(K(e) - E(e)), \tag{3}$$

$$B = (p_0/E^*)(b/e^2a^2)\left(\frac{a^2}{b^2}E(e) - K(e)\right), \tag{4}$$

and

$$\delta = \frac{bK(e)}{E^*}(p_0 + 2p_1), \tag{5}$$

where δ, the overall relative displacement of the two contact bodies, equals the displacement of the asperity peak. A and B $(A < B)$ are the principal radii of curvature of the asperity. $K(e)$ and $E(e)$ are the complete elliptic integrals of the first and the second kind of the argument $e = (1 - b^2/a^2)^{1/2}$, $b < a$ [8]. E^* is the combined stiffness $\frac{1}{E^*} = \frac{1-v_1^2}{E_1} + \frac{1-v_2^2}{E_2}$, E_1 and E_2 are Young's moduli of the surfaces, and v_1 and v_2 are the corresponding Poisson's ratios. A

combination of Equations (3) and (4) gives

$$Aa^2 + Bb^2 = \frac{p_0 b}{E^*} K(e). \tag{6}$$

Equations (3) and (4) show that the ratio of the large and small radii, $\lambda = b/a$, is independent of external load and is determined by

$$\frac{B}{A} = \frac{E(e) - \lambda^2 K(e)}{\lambda^2 [K(e) - E(e)]}, \tag{7}$$

where $\lambda = b/a$ and $b \leq a$. The elastic strain energy stored in the contact bodies can be estimated from Equations (1), (2), and (5):

$$\begin{aligned} U_E &= \int\int_{(x,y)\in\Omega} p(x,y)U(x,y)\,dx\,dy \\ &= \pi a^2 \left\{ \frac{bK(e)}{E^*} \left(\frac{1}{3}p_0^2 + \frac{5}{3}p_0 p_1 + 2p_1^2 \right) - (Aa^a + Bb^2) \left(\frac{1}{15}p_0 + \frac{1}{3}p_1 \right) \right\}. \end{aligned} \tag{8}$$

For spheres, $a = b$ and $K(e) = \pi/2$. The corresponding strain energy is [9]

$$U_E = \frac{\pi^2 a^3}{E^*} \left(\frac{2}{15}p_0^2 + \frac{2}{3}p_0 p_1 + p_1^2 \right). \tag{9}$$

The following relations can be found from Equations (3) and (4):

$$p_0 = \frac{Aa^2 + Bb^2}{bK(e)} E^* \tag{10}$$

and

$$p_1 = \frac{\delta - Aa^2 - Bb^2}{2bK(e)} E^*. \tag{11}$$

The strain energy as a function of the displacement, δ, can be derived by substituting Equations (10) and (11) into Equation (9):

$$U_E = \frac{\pi a E^*}{2\lambda K(e)} \left(\frac{1}{5}\beta^2 a^4 - \frac{2}{3}\beta\delta a^2 + \delta^2 \right), \tag{12}$$

where $\beta = A + \lambda^2 B$. Variation in strain energy, U_E, with a and b can be determined, keeping $\lambda = b/a$ and the overall relative displacement of

the two contact bodies constant (the elliptical shape of the contact area does not change). It is easy to find from Equation (12) that

$$\left.\frac{\partial U_E}{\partial a}\right|_{\delta,\lambda} = \frac{\pi E^*}{2\lambda K(e)}\left[\beta a^2 - \delta\right]^2 = \frac{2\pi\lambda a^2 K(e)}{E^*} p_1^2. \tag{13}$$

For spheres, $\beta = 1/R$, where R is the radius of the sphere. Equation (13) becomes $\frac{\partial U_E}{\partial a}|_{\delta} = \frac{\pi^2 a^2}{E^*} p_1^2$ [9].

The free surface energy due to adhesion can be modeled as:

$$U_S = -2\gamma\pi ab, \tag{14}$$

where 2γ is the combined surface energy per unit area of two surfaces and πab is the contact area. For a sphere, the free surface energy is $U_S = -2\gamma\pi a^2$ [9]. The total energy of the system is $U_T = U_E + U_S$. For equilibrium, $\partial U_T/\partial a$ vanishes, giving

$$\left[\beta a^2 - \delta\right]^2 = \frac{8\lambda^2 K(e) a\gamma}{E^*}. \tag{15}$$

Using the relationship given by Equation (11), an expression for p_1 can be found:

$$p_1 = -\left[\frac{2\gamma E^*}{aK(e)}\right]^{1/2}. \tag{16}$$

On the other hand, the integration of Equation (1) over the contact area, Ω, gives the total contact force:

$$P = 2\pi\lambda a^2\left(\frac{p_0}{3} + p_1\right). \tag{17}$$

Combining Equations (16) and (17), a relationship regarding the external load can be found:

$$\left[P - \frac{2\pi\beta E^* a^3}{3K(e)}\right]^2 = \frac{8\pi^2\gamma\lambda^2 E^* a^3}{K(e)}. \tag{18}$$

For a sphere, Equation (18) becomes

$$\left[P - \frac{4E^* a^3}{3R}\right]^2 = 16\pi\gamma E^* a^3, \tag{19}$$

which is the fundamental equation for the JKR theory. The variables a, δ, and P can be made dimensionless as $a^* = a/a_c$, $\delta^* = \delta/\delta_c$, and $P^* = P/P_c$. The following parameters can be used in nondimensionalization:

$$a_c = \left(\frac{9\gamma\lambda^2 K(e)}{2\beta^2 E^*}\right)^{1/3}, \tag{20}$$

$$\delta_c = \left(\frac{9\gamma\lambda^2 K(e)}{2\beta^{1/2} E^*}\right)^{2/3}, \tag{21}$$

and

$$3P_c = \frac{2\pi\gamma\lambda^2}{\beta}. \tag{22}$$

Using these expressions, Equations (15) and (18) can be nondimensionalized as

$$(\delta^* - a^{*2})^2 = \frac{16}{9}a^* \tag{23}$$

and

$$(P^* - a^{*3})^2 = 4a^{*3}. \tag{24}$$

Equations (23) and (24) constitute the generalized JKR model valid for all parabolic contact. The JKR model for a sphere is one of the special cases of these equations.

The predicted contact behavior of the generalized JKR model for an arbitrarily shaped parabola is shown in Figures 2, 3, and 4. Figure 2 depicts the relationship between the longer radius of the contact area and the overall displacement according to both the Hertzian and JKR theories. Hertzian theory shows a monotonic relationship between these two variables. No contact area is formed when the surfaces are separated. However, for JKR theory, the adhesion between surfaces can develop at a relatively low tensile stress. Therefore, the contact area starts to appear even when the overall displacement is negative. The relationship between the overall displacement and the longer radius of the contact area is not monotonic. As shown in Figure 2, no contact occurs when the approaching distance between the contact bodies is larger than the critical distance ($-\delta^* > (1/3)^{1/3}$). However,

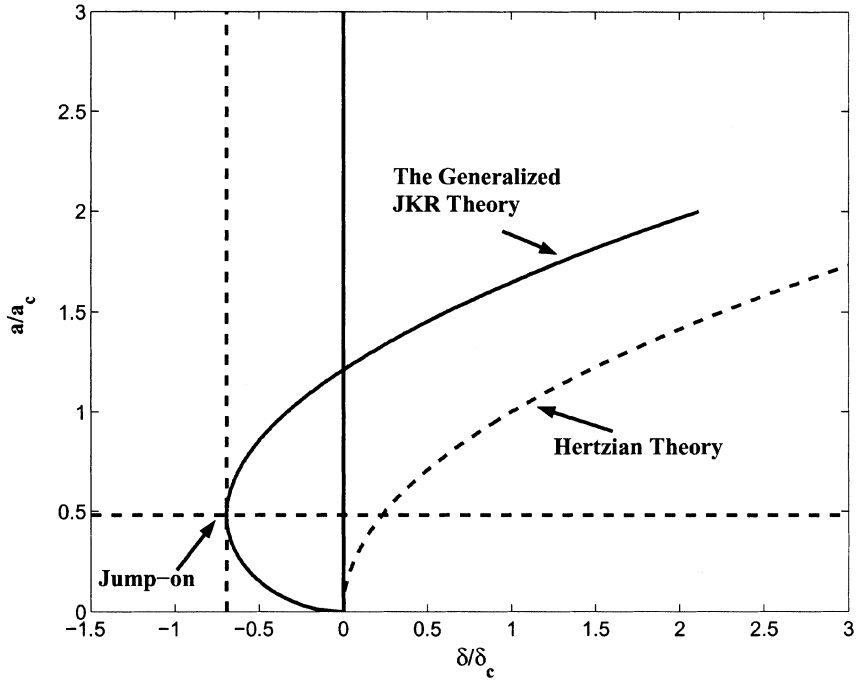

FIGURE 2 a/a_c versus δ/δ_c for a single asperity.

due to adhesion, the contact bodies make a sudden contact when they are at the critical distance $-\delta^* = (1/3)^{1/3}$. The sudden establishment of the contact is called "jump-on." A contact area with the longer radius of $a^* = (1/3)^{2/3}$ is formed at the jump-on. Multiple solutions exist when the distance between the contact bodies is smaller than the critical distance $(0 \leq -\delta^* \leq (1/3)^{1/3})$. When multiple solutions exist, the larger contact area is the stable solution that is observed in reality.

Figure 3 displays the relationship between the external load and the longer contact radius. Again, Hertzian theory predicts a monotonic relationship and the JKR theory predicts multiple solutions at $-1 \leq P^* \leq 0$. When multiple solutions exist, the larger contact area is the stable solution. Therefore, $P^* = -1$ is the turning point. Two contact bodies suddenly are separated and the contact area becomes zero when the dimensionless pull-off force is larger than or equal to unity. Figure 4 shows the displacement-load relationship. The stable-solution branch will be used in modeling rough surface contact, which is introduced in the following section.

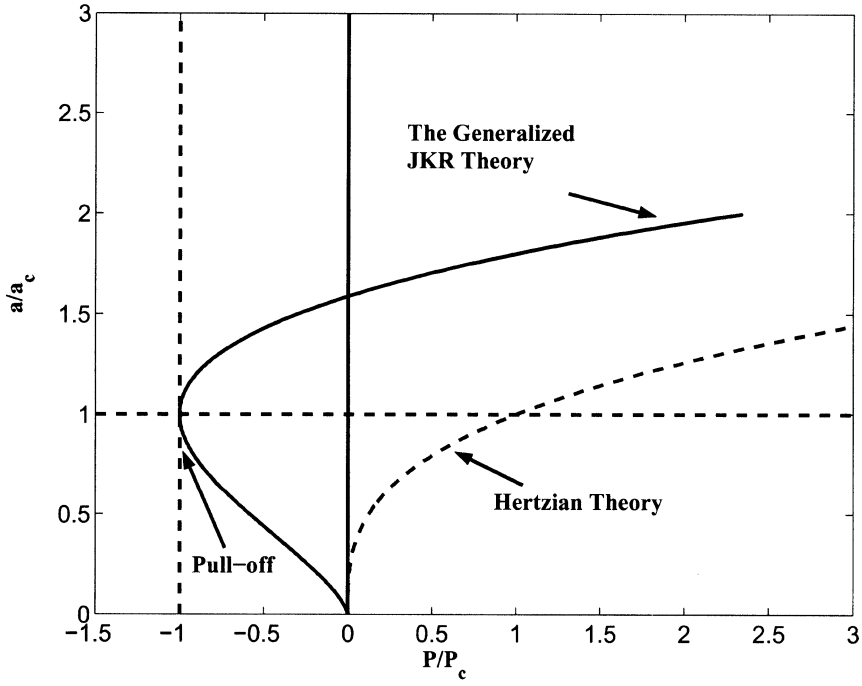

FIGURE 3 a/a_c versus P/P_c for a single asperity.

Rough Surface Reconstruction

The next step in formulating the rough-surface contact model is to describe analytically the surface heights of the rough surface. The rough surface is modeled as the superposition of parabolics with arbitrary principal radii of curvature and orientation. For the region used to characterize the rough surface, an asperity peak is defined as any point at which the local slope of the surface is zero and the height is higher than neighboring points. In other words, the asperity peaks are local maxima. Therefore, the local surface surrounding a particular asperity peak at (x_0, y_0) can be described by

$$S(x - x_0, y - y_0) = A_0 x^2 + B_0 y^2 + C_0 xy. \tag{25}$$

Equation (25) is digitized in a discrete form, which is suitable for image analysis of an AFM surface image:

$$K(i,j) = Ai^2 + Bj^2 + Cij, \tag{26}$$

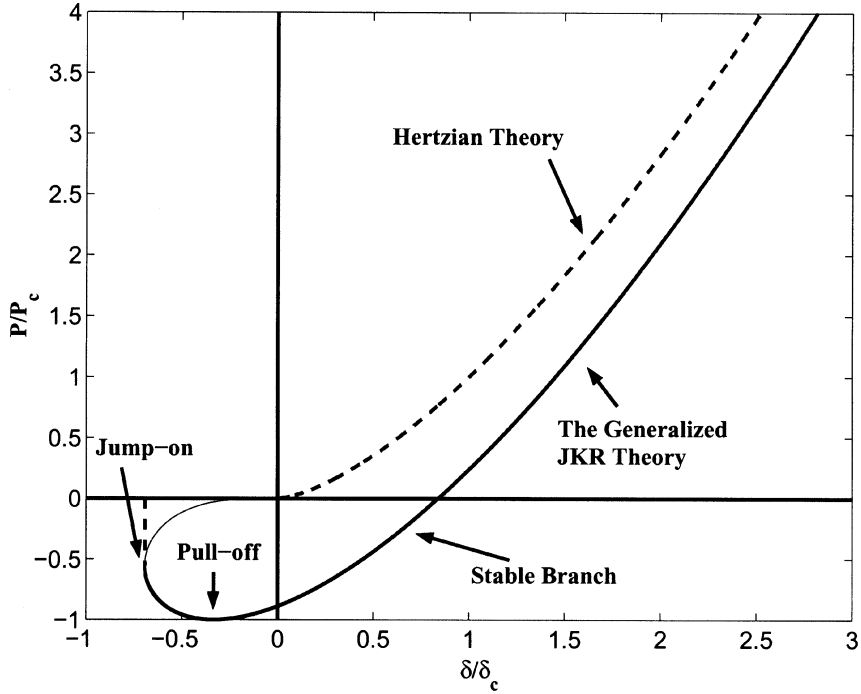

FIGURE 4 The nondimensional load-displacement relationship for a single asperity.

where (i,j) is the relative distance between neighboring points and the peak point. The coefficients A, B, and C relate to A_0, B_0, and C_0 by

$$A_0 = A\xi, \tag{27}$$

$$B_0 = B\xi, \tag{28}$$

$$C_0 = C\xi, \tag{29}$$

and

$$\xi = \frac{dz}{dx^2}, \tag{30}$$

where dx is the resolution of one pixel of the AFM image (with units of nm/pixel) and dz is the surface height resolution of the AFM image. For the AFM data used in this study, surface heights within the range of 0 to 23 nm are represented by 221 units. Therefore, $dz = 0.1\,\text{nm}$. Coefficients A, B, and C then can be determined by a least-squares

regression analysis of the heights of neighboring points (in this study, surface heights within a 5×5 square centering at the peak are used). For convenience, the local surface near the asperity peak is described in the new axis system by rotation of the principal axes so that:

$$S(\hat{i},\hat{j}) = \hat{A}\hat{i} + \hat{B}\hat{j}, \tag{31}$$

where $\hat{A}$ and $\hat{B}$ are the principal radii of curvature and $\hat{A} \leq \hat{B}$. It is easy to show that the orientation angle of the principal axes is

$$\hat{A} = A\cos^2\theta + B\sin^2\theta + C\cos\theta\sin\theta, \tag{32}$$

$$\hat{B} = A\sin^2\theta + B\cos^2\theta - C\cos\theta\sin\theta, \tag{33}$$

and

$$\theta = \frac{1}{2}\arctan\frac{C}{A-B}. \tag{34}$$

Obviously, for real surfaces there is no guarantee that $\hat{A} = \hat{B}$. The statistical characteristics of the orientation of the principal axes and the principal radii of curvature are summarized in the following section. Finally, the extracted radii of curvature and orientation angles can be used to reconstruct the asperity. The rough surface then is reconstructed by the superposition of individual asperities (by hiding the overlapping parts).

Superposition of Asperity Contacts

Based on the results of surface reconstruction and single-asperity contact modeling, the contact between a rough surface and a smooth sphere can be modeled. At first, an overall displacement of the sphere, δ_0, is specified. The distance between each asperity peak and the surface of the sphere is calculated as:

$$\delta_i = Z_{max} - Z_i + S_i - \delta_0, \tag{35}$$

where Z_{max} is the height of the peak that makes the first contact with the surface of the sphere. Z_i is the height of the ith peak. S_i is the height of the point on the sphere that contacts the ith peak. The displacement, δ_i, is then nondimensionalized by $\delta_i^* = \delta_i/\delta_{ci}$. The parameter δ_{ci} that nondimensionalizes an asperity's displacement is calculated from Equation (21) by using corresponding values of λ and β acquired from the surface reconstruction procedure. When $d_i^* \geq -(1/3)^{1/3}$, the dimensionless contact force, P_i^*, is determined

from the generalized JKR relationship shown in Figure 4. When $d_i^* < -(1/3)^{1/3}$, the contact force vanishes, $P_i^* = 0$. The total contact force over the simulated area then is computed by the summation of individual contact forces by $P = \Sigma_i P_i^* P_{ci}$. The factor P_{ci} is defined by Equation (22) with λ and β associated with the ith asperity peak. In the present study, contact-region overlapping is neglected. The possible error caused by this approximation is discussed in the following section.

DIRECT SIMULATION MODEL

The second method for rough surface contact modeling is the direct-contact simulation model based on the half-space elastic theory. In the absence of adhesion, it is not necessary to use asperity-superposition models. Contact can be simulated directly based on the half-space elastic theory.

In this section the equations used to describe the load-displacement equations for two bodies in contact are introduced. The two bodies are compressed in the normal direction. The surfaces of the two bodies are assumed to be frictionless. In this case, deformation in the tangential directions does not contribute to the normal displacement. By combining the displacement and material properties of both bodies, the normal displacement of contact according to the half-space assumption can be obtained as

$$U(x,y) = \frac{1}{2\pi}\left(\frac{1-\mu_1}{G_1} + \frac{1-\mu_2}{G_2}\right)\int_\Omega \frac{dS}{r}, \tag{36}$$

where $r = \sqrt{(x-x')^2 + (y-y')^2}$ and $dS = dx'dy'$. $U(x,y)$ represents the normal displacement at point (x,y). The contact stiffness is $G_i = E_i/(2+2\mu_i)$. The separation between the surfaces of the two bodies is related to the normal displacement, $U(x,y)$, the combined surface heights, $S(x,y)$, and overall relative displacement, δ_0, of two bodies in contact by:

$$h(x,y) = -U(x,y) + S(x,y) - \delta_0, \tag{37}$$

where $h(x,y)$ represents the separation between two surfaces and

$$S(x,y) = Z_{max} - Z(x,y) + S_0(x,y). \tag{38}$$

$Z(x,y)$ represents the rough surface height, Z_{max} represents the highest peak that makes first contact with the sphere, and $S_0(x,y)$

represents the height of the sphere's surface. Over the contact region, the two surfaces contact each other and $h(x,y) = 0$. Outside the contact region where $h(x,y) > 0$, the surfaces are separated and no interaction exists between them. Therefore, the surface stress, $\sigma(x,y)$, is zero. This constraint, however, is valid only for elastic contact. Hence, the approach described in this section is not suitable for adhesive contact simulation.

The integral in Equation (36) can be calculated by dividing the contact area into uniform square meshes with constant pressure distributed inside each of the elements. The load-displacement can be expressed in the discrete form as:

$$U(i,j) = \sum_{m=1}^{M} \sum_{n=1}^{N} A_{ij,mn} \sigma_{mn}, \tag{39}$$

with $1 \le i,m \le M$ and $1 \le j,n \le N$. The coefficient $A_{ij,mn}$ represents the displacement at point (i,j) produced by the pressure at (m,n). It can be calculated by [7]

$$A_{ij,mn} = \frac{dx}{2\pi} \left(\frac{1-\mu_1}{G_1} - \frac{1-\mu_2}{G_2} \right) (A_1 + A_2), \tag{40}$$

where

$$A_1 = a_1 \ln \frac{b_1 + \sqrt{a_1^2 + b_1^2}}{b_2 + \sqrt{a_1^2 + b_2^2}} - a_2 \ln \frac{b_1 + \sqrt{a_2^2 + b_1^2}}{b_2 + \sqrt{a_2^2 + b_2^2}} \tag{41}$$

and

$$A_2 = b_1 \ln \frac{a_1 + \sqrt{a_1^2 + b_1^2}}{a_2 + \sqrt{a_2^2 + b_1^2}} - b_2 \ln \frac{a_1 + \sqrt{a_1^2 + b_2^2}}{a_2 + \sqrt{a_2^2 + b_2^2}}. \tag{42}$$

Here $a_1 = m - i + 0.3$, $a_2 = a_1 - 1$, $b_1 = n - j + 0.5$, and $b_2 = b_1 - 1$. The contact pressure and displacement can be found using a simple and effective algorithm introduced by Kalker [6, 7]. The algorithm guarantees the convergence of the solution by forcing the boundary condition that over the contact area $(i,j \in \Omega)$, $\sigma_{ij} > 0$, and $h(i,j) = 0$, and outside the contact area $(i,j \notin \Omega)$, $\sigma_{ij} = 0$ and $h(i,j) > 0$. The rough surface itself does not need to be reconstructed. The surface height data from the AFM image can be used directly as the input for $Z(x,y)$ given by Equation (38).

Using the direct simulation model, the contact between a smooth sphere and a smooth flat surface can be calculated. The radius of the sphere is 3 μm. The Young's modulus and Poisson's ratio for the

material are 75 GPa and 0.22, respectively. Figure 5 shows that the results on the displacement-load relationship from the direct numerical simulation agree very well with the analytical expression from the Hertzian theory. The largest difference between the numerical simulation and the Hertzian theory is less than 1%. The direct simulation model for elastic contact gives a very accurate solution that can be used to compare with the results from the asperity-superposition model. By comparing results of these two kinds of approaches, the validation and accuracy of the asperity-superposition model can be evaluated.

Detailed results on surface displacement and contact pressure can be derived as shown in the following section. However, the method has difficulty in simulating adhesion based on surface energy. A new constraint and searching method is needed to include the effects of surface energy. This constraint can be a model that relates separation with adhesion, such as the Dugdale model, the Lennard-Jones model, or a quadratic-programming method used to find multiple solutions.

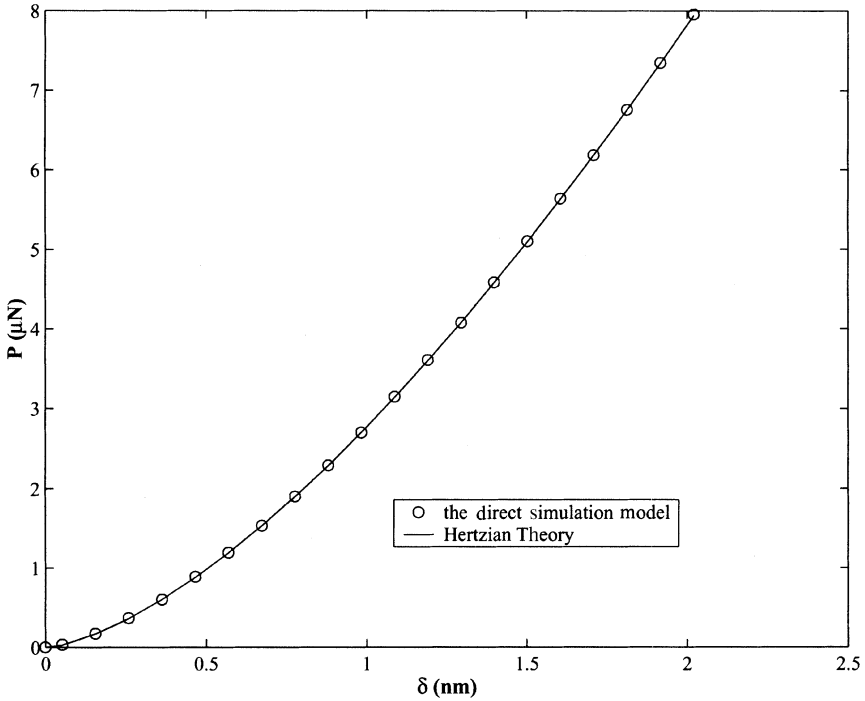

FIGURE 5 The displacement-load relationship from the direct simulation and Hertzian theory.

SIMULATION RESULTS AND COMPARISONS

Basic Simulation Parameters

The modeling methods described in the previous sections are used to simulate the contact between a glass sphere and a rough glass surface. Young's modulus of the material is 75 GPa and the Poisson's ratio is 0.22. Free surface energy is important in the adhesion calculation. However, the surface energy for glass differs over a wide range. In the current study, Gilman's equation from the elementary theory was used to estimate the surface energy [10]:

$$\gamma = (E/y_0)(a_0/\pi)^2, \tag{43}$$

where γ is the surface energy, y_0 is the distance between the crystallographic cleavage planes, and the a_0 value is taken to equal the atomic radii of atoms lying in the cleavage planes. Usually $y_0 = 2$ Å and $a_0 = 1.3$ Å. Experiments show that the elementary theory (Equation (43)) gives a relatively reasonable prediction for the surface energy based on the Young's modulus [10].

The surface heights of the glass surface are acquired by an AFM scan, as shown in Figure 6. The actual area of the AFM scan is 5×5 μm. The glass surface has a roughness range of 23 nm. The pixel resolution of the AFM scan is $dx = 9.77$ nm/pixel. The resolution on height is $dz = 0.1$ nm. The surface of the glass sphere is assumed to be smooth. The radius of the sphere is 3 μm.

The glass surface is divided into 8×8 subareas, as shown in Figure 7. Centers of the subareas are selected as the centers of contact between the smooth sphere and the surface. Therefore, 64 cases are simulated and the statistical properties of the contact position are analyzed.

Surface Reconstruction Results

Surface features of the glass surface such as the heights, orientation, and ratios of the longer to shorter radii of the asperities can be extracted. The rough surface is reconstructed by the superposition of individual asperities.

Figure 8 shows the reconstructed surface of the glass. The root-mean-square difference between the original roughness height (shown in Figure 6) and the reconstructed surface height (shown in Figure 8) is 0.0034 nm, about 0.03% of the original mean surface height. The other two parameters, the roughness average, R_a, and the root means square average, R_q, are also used in describing the reconstructed and

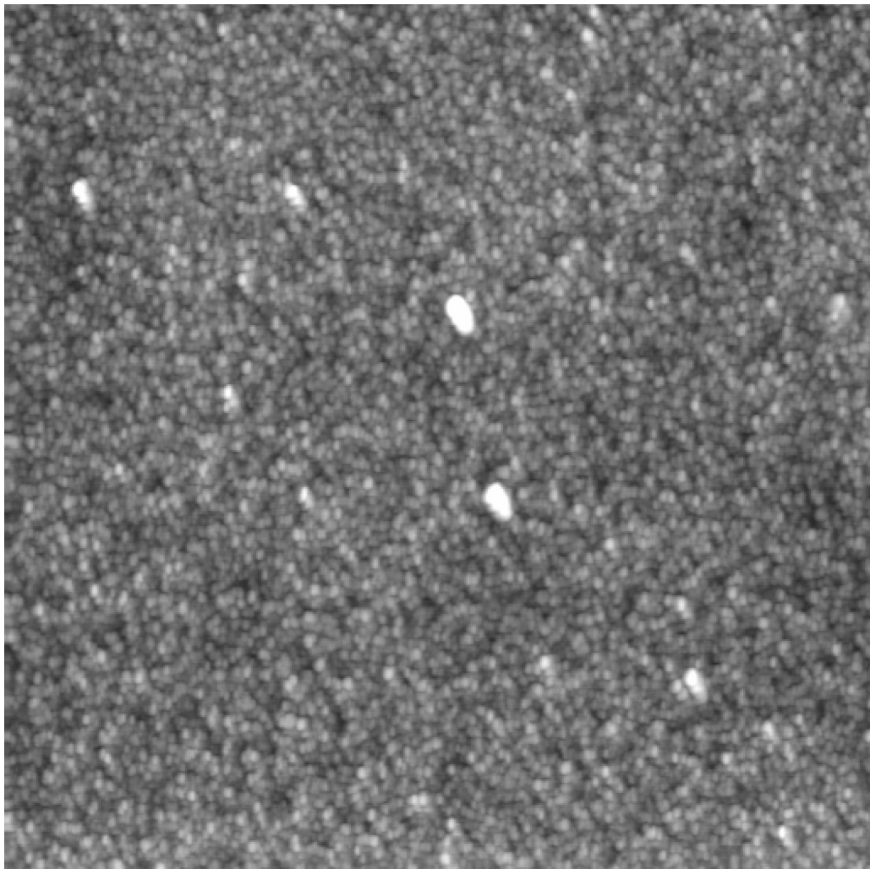

FIGURE 6 The AFM image of the glass surface.

the original surfaces. The definitions of R_a and R_q are:

$$R_a = \frac{1}{M \times N} \sum_{i=1}^{M} \sum_{j=1}^{N} |Z_{ij} - \bar{Z}|, \tag{44}$$

$$R_q = \sqrt{\frac{1}{M \times N} \sum_{i=1}^{M} \sum_{j=1}^{N} (Z_{ij} - \bar{Z})^2}, \tag{45}$$

where M and N are numbers of data points in x and y, Z_{ij} is the surface height relative to the datum plane, and $\bar{Z}$ is the height of the datum plane. In the current surface regression method, $\bar{Z} = 0$. The R_a of the original and the reconstructed surfaces are 12.842 nm and 12.880 nm, respectively. The difference in R_a between the reconstructed

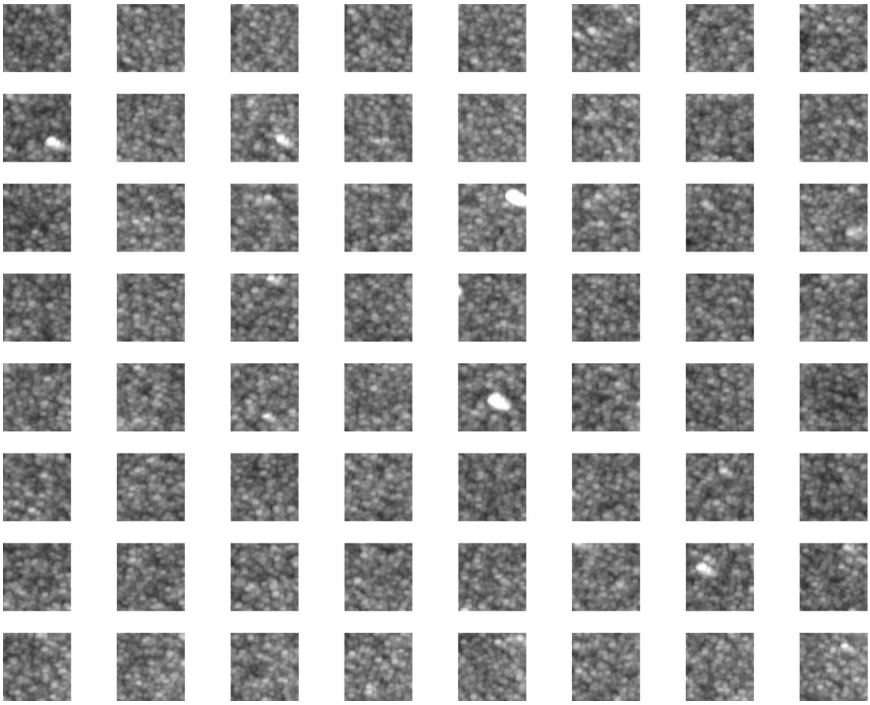

FIGURE 7 8×8 simulated contact areas.

and the original surfaces is 0.30%. The R_q of the original and the reconstructed surfaces are 0.0253 nm and 0.0256 nm, respectively. The difference, R_q, between the reconstructed and the original surfaces is 1.14%. Another commonly accepted parameter, R_z, the average maximum profile of the ten greatest peak-to-valley separations, is not used in the current comparison because in the parabolic least-square surface regression method only the peaks are matched. The valleys, which do not contribute to the contact, are not considered. The above results show that the current surface model represents the original rough surface very well. This provides a validation of the surface feature extraction method.

Figure 9 shows the statistical properties of the asperity peaks. The probability distribution of the heights of the asperity peaks, Z, is concentrated in two groups. The group near 15 nm follows a Gaussian distribution. The other group near 27 nm includes all the highest peaks. It corresponds to the bright spots in Figures 6 and 8. These high peaks may be contaminant microparticles that were not removed by cleaning. The peak of the probability distribution function of $\ln B/A$

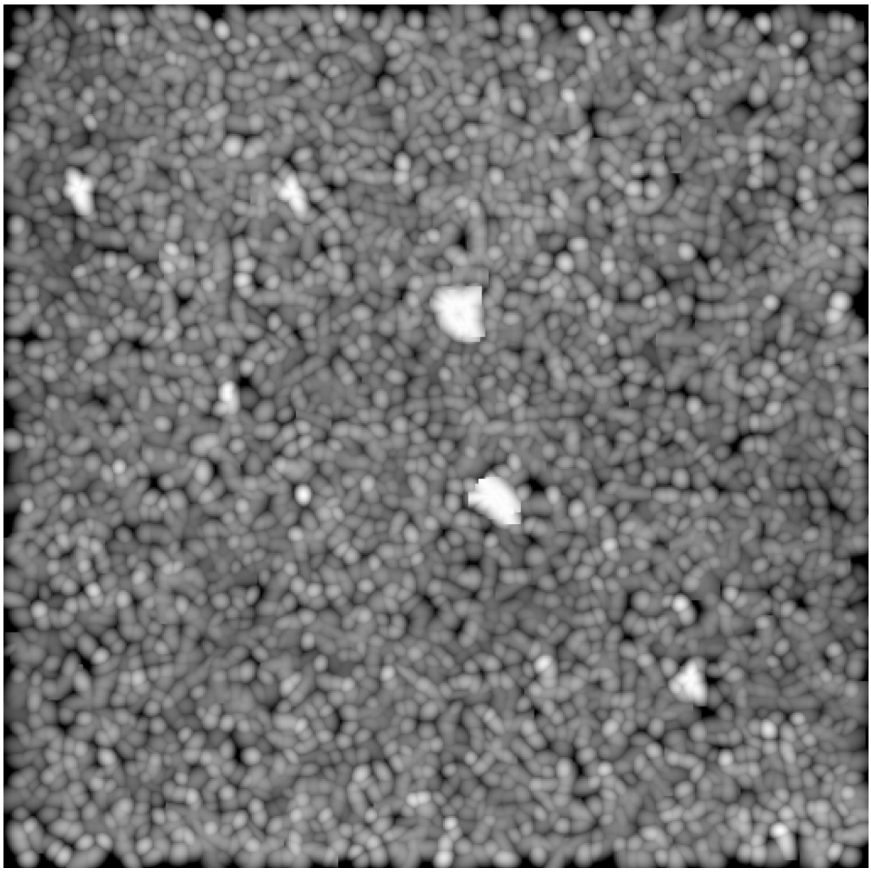

FIGURE 8 The reconstructed glass surface.

(A and B are defined in Equations (3) and (4)), is biased toward zero. Most asperities have a longer radius that is less than 10 times the shorter radius. Figure 9 also shows the distribution of $\lambda = b/a$, the ratio of the shorter-to-longer radii of the contact area (a and b are shown in Figure 1). The mean value of λ is 0.6. This implies that most contact regions are elliptic. The distribution of λ can be approximated by a Gaussian distribution without introducing severe errors. The probability distribution of the orientation angles of the principal axes of the asperities is relatively uniform. No directional preference is observed. The results collectively support that this is an effective way to determine asperity-related parameters and statistics.

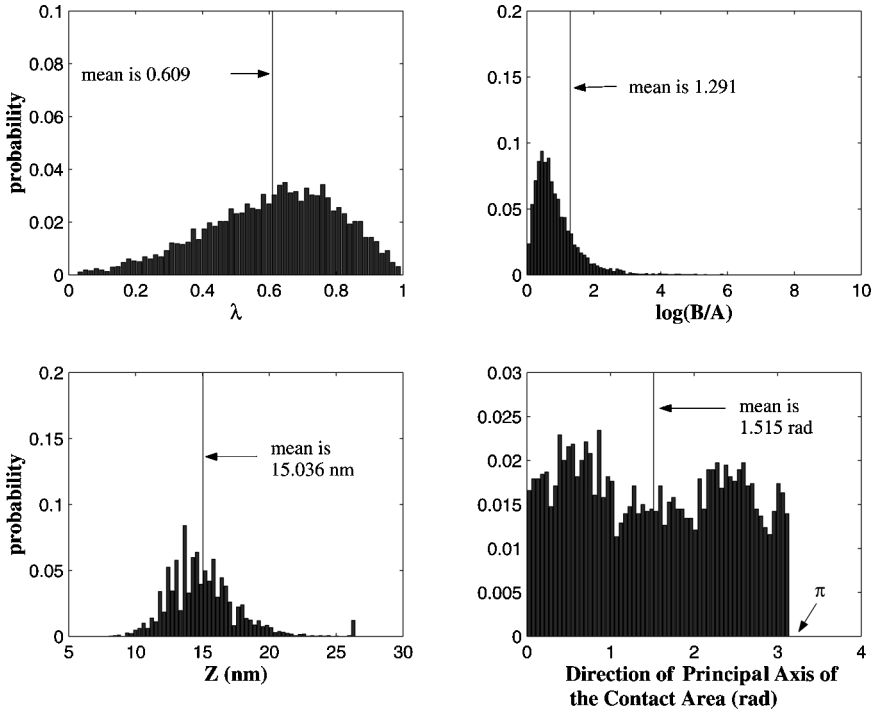

FIGURE 9 Statistics of the reconstructed glass surface.

Direct Simulation Results

Contact simulations can be performed using the direct-simulation and asperity-superposition models in parallel. The contacts of a smooth sphere with each of the 64 subregions shown in Figure 7 can be simulated to analyze the effects of the locations of the contact areas.

Figures 10, 11, and 12 show the results of the direct simulation model. Figure 10 displays the contact pressure and displacement of the surface when the overall displacement is approximately 17 nm. The contact regions overlap. The contact pressure not only causes deformation over the contact area but also displacement in the outside region. The interaction between individual asperity peaks implies that the asperity superposition method is not accurate when the overall displacement, δ_0, is large. Figure 11 shows the displacement-load relationship at $\delta_0 = 5.08$ nm. Because of surface roughness, the displacement-load relationship varies for each of the 8×8 contact locations. At $\delta = 5.08$ nm, the probability of contacts between the sphere and

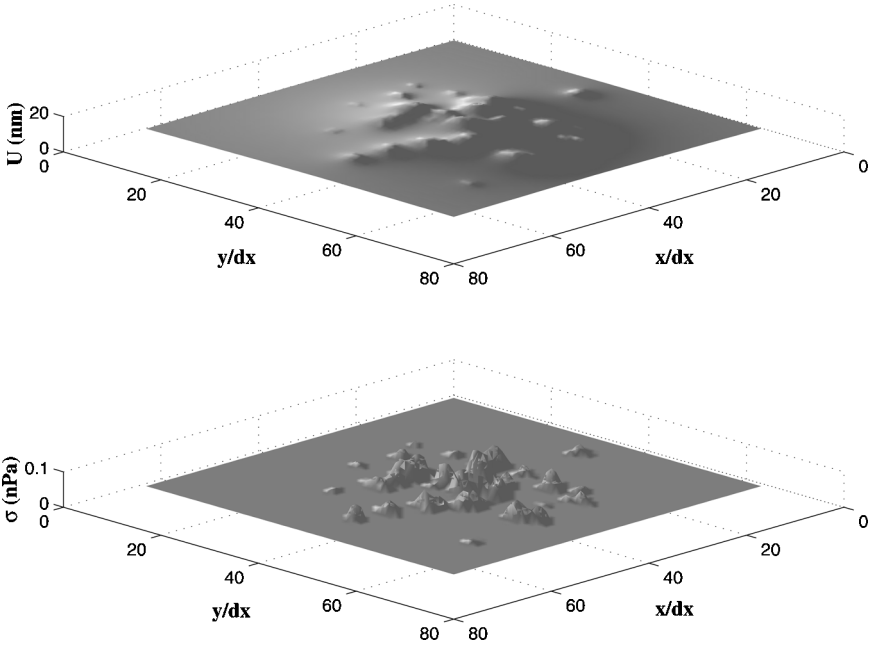

FIGURE 10 The contact pressure and displacement of a smooth sphere in contact with a rough glass surface.

the rough surface is low. The mean contact force for the 64 subregions is 0.4 μN. The standard deviation is 3 μN. The secondary peak of probability near 20 μN reflects the higher contact forces that can be produced if the center of the sphere is near some of the surface's highest spots (where the surface is contaminated by debris particles). The high spots have significant effects on the standard deviation of the contact forces. As a result, the standard deviation is 10 times as great as the mean. It is clear that the probability distribution function of the surface contact force is affected not only by the roughness of the surface but also by the overall displacement and whether or not the surface is clean. The distribution is extended as the overall displacement increases, which brings the sphere closer to the rough surface as shown in Figure 12. When $\delta = 15.4$ nm, the probability for contact increases and the probability of contact force is extended. The mean is 21 μN and the standard deviation is 11 μN. A secondary peak appears near 80 μN, corresponding to the effects of the contaminant microparticles that are attached to the rough surface.

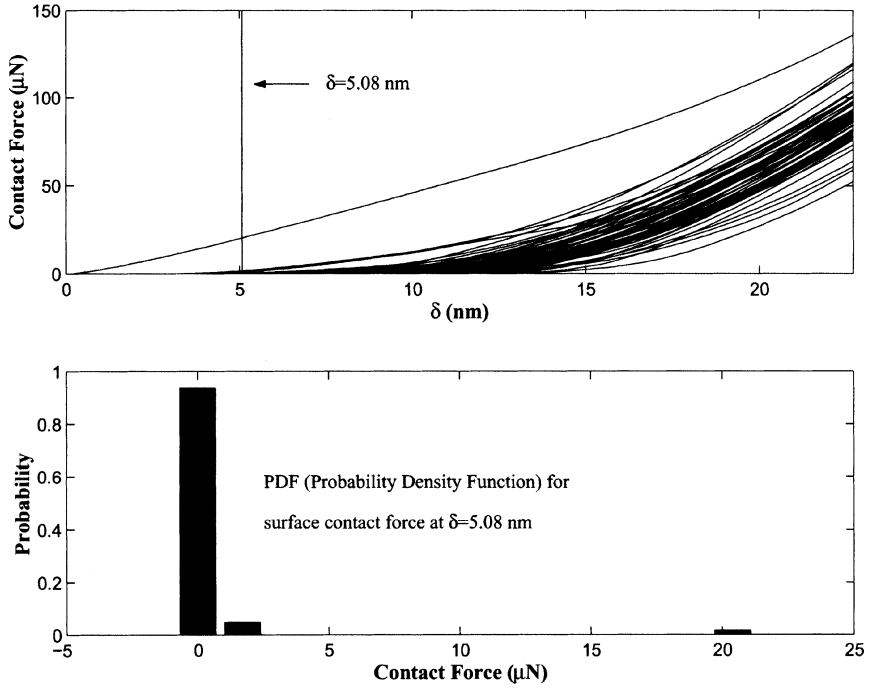

FIGURE 11 The overall load-displacement relationship at $\delta = 5.08\,\text{nm}$.

Figure 13 displays the mean displacement-load relationship for the rough-surface contact. Surface roughness significantly reduces the contact force. However, it is hard to make a comparison between the rough-surface and smooth-surface cases. This is because the overall height of a rough surface is not defined uniquely. For a smooth surface, at zero displacement, the sphere begins to contact the flat surface. However, multiple heights can be used as the datum in measuring the overall surface displacement. In the current simulation, the datum for zero displacement is defined as the top plane of the highest peak of the rough surface. For small displacements, very few asperity peaks are in contact with the sphere. Consequently, the contact area is reduced significantly. As a result, the ratio of the rough-surface to smooth-surface contact forces is less than 0.1 for $\delta < 10\,\text{nm}$, as shown in Figure 13. In other words, there is a very significant reduction in the contact force at small displacements because of surface roughness. As the overall displacement increases, the rough-surface contact force

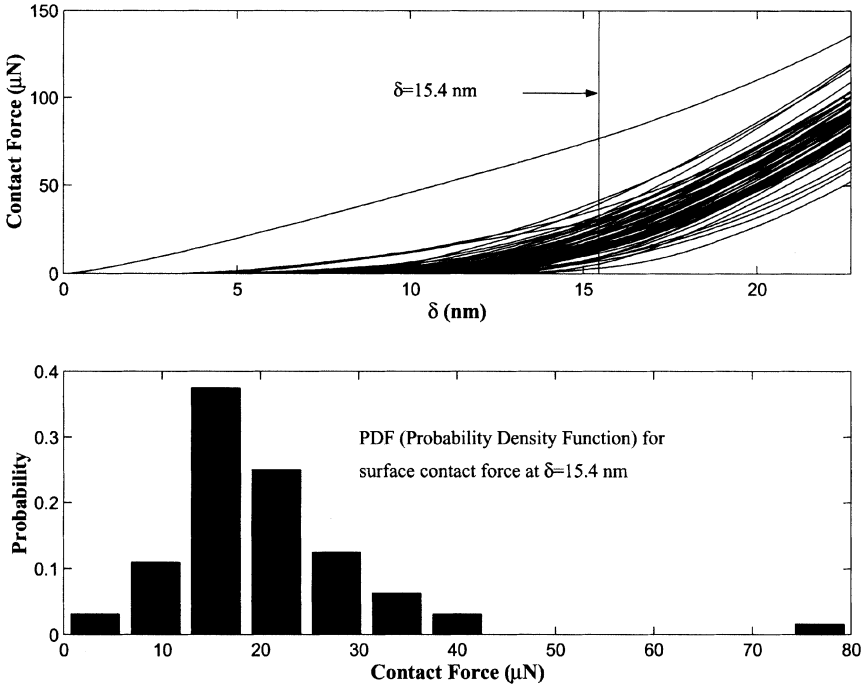

FIGURE 12 The overall load-displacement relationship at $\delta = 15.4$ nm.

increases to about 25% of the smooth contact force for the same displacement.

Asperity-Superposition Results

The advantage of the asperity-superposition approach is that it provides a way to model the adhesive contact between the rough surface and the smooth sphere by the generalized JKR theory. However, one drawback is that the method is valid only for cases when the external load and overall displacement are small. At a higher load, the overlapping of contact regions is possible, as indicated by the direct simulation results described in the previous section. However, the direct-simulation and asperity-superposition models can be performed in parallel for the case of pure-elastic contact. By comparing the results from both methods, it can be determined when the asperity-superposition is valid.

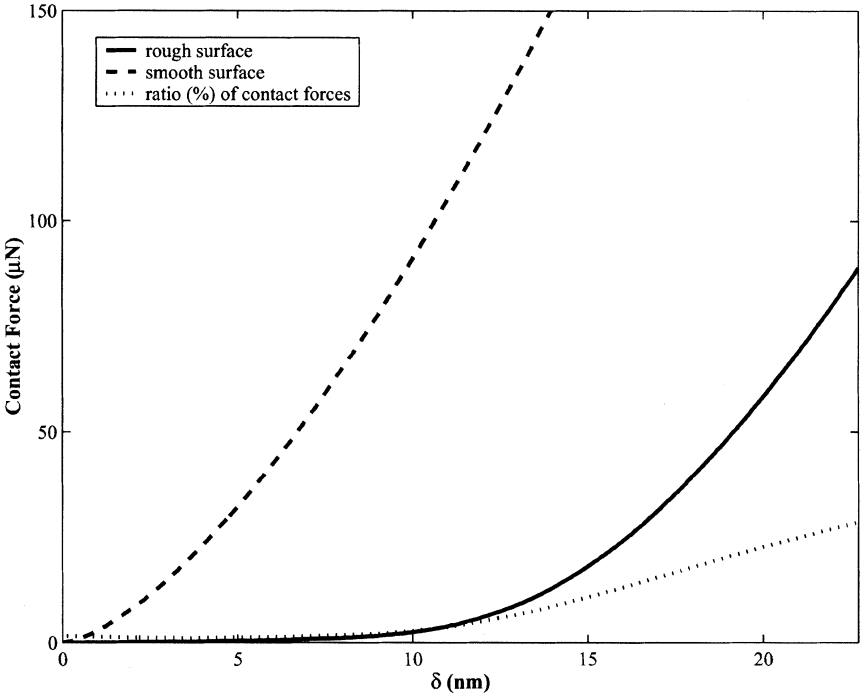

FIGURE 13 The mean overall displacement-load relationship.

Figure 14 displays the load-displacement relationship for pure elastic contact between the sphere and 58 of the 64 subregions that were predicted by the direct-simulation method and the asperity-superposition method. The results for subregions with large high spots were not included in the curves. When $\delta_0 \geq 12$ nm, the difference between both methods increases dramatically. When the overall displacement is small, the asperities do not interact with each other during deformation and the contact regions do not overlap. Therefore, when $\delta_0 < 12$ nm, both methods give similar results.

Adhesive contact between the smooth sphere and each of the 64 subregions of the rough surface also can be simulated with the asperity-superposition model. Figure 15 shows the load-displacement relationship for one of the subregions by the Hertzian theory and the asperity superposition model. The external force is negative when $9.8 < \delta_0 \leq 1.24$. The pull-off force is -8.6 μN and the pull-off force for the smooth surface is -19.1 μN. Thus, the pull-off force is reduced to approximately 50% because of surface roughness. Figure 15 also

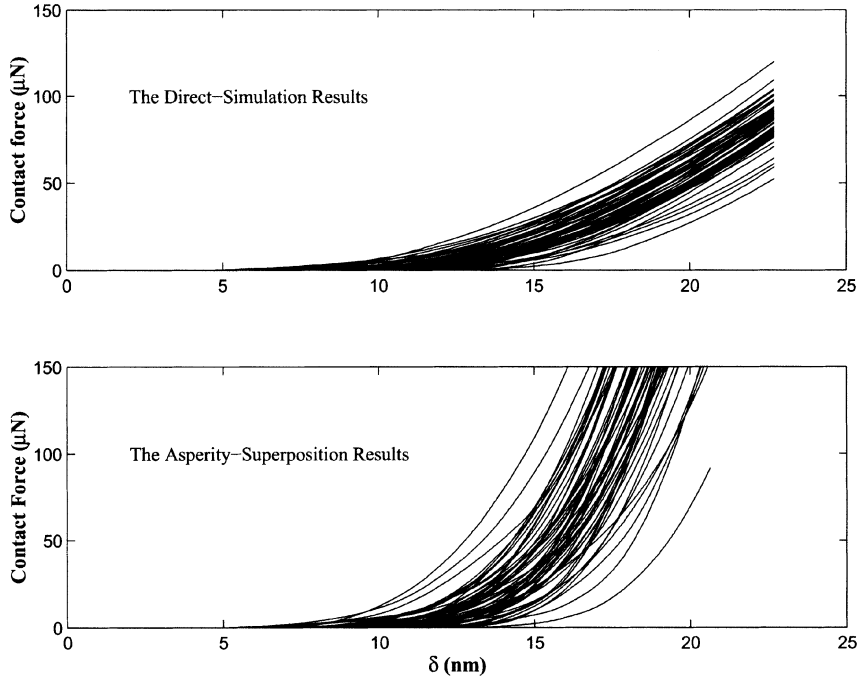

FIGURE 14 The load-displacement relationship for rough surface contact.

reveals that when $\delta_0 \geq 18$ nm, the contact force for rough-surface contact surpasses that for smooth-surface contact. This is unrealistic. When δ_0 is larger than 15 nm, the deformation of the two surfaces and the overlapping and merging of contact regions must be taken into account.

Figure 16 shows the distribution of pull-off force magnitudes. The mean magnitude of the pull-off force is 2.0 μN, approximately 10% of the pull-off force of the smooth contact. Supportive data for the significant reduction of adhesion due to surface roughness can be found in Kim *et al.* [11], Soltani [12] and the recent experimental work of Ibrahim *et al.* [13]. The standard deviation of the pull-off force is 1.37 μN. The mean overall pull-off displacement is 9.7 nm. The standard deviation of the pull-off displacement is 2.52 nm. The mean pull-off displacement is smaller than 12 nm. At the pull-off displacement, no significant effects of contact region overlap need to be considered. The asperity superposition method is valid in computing the pull-off force.

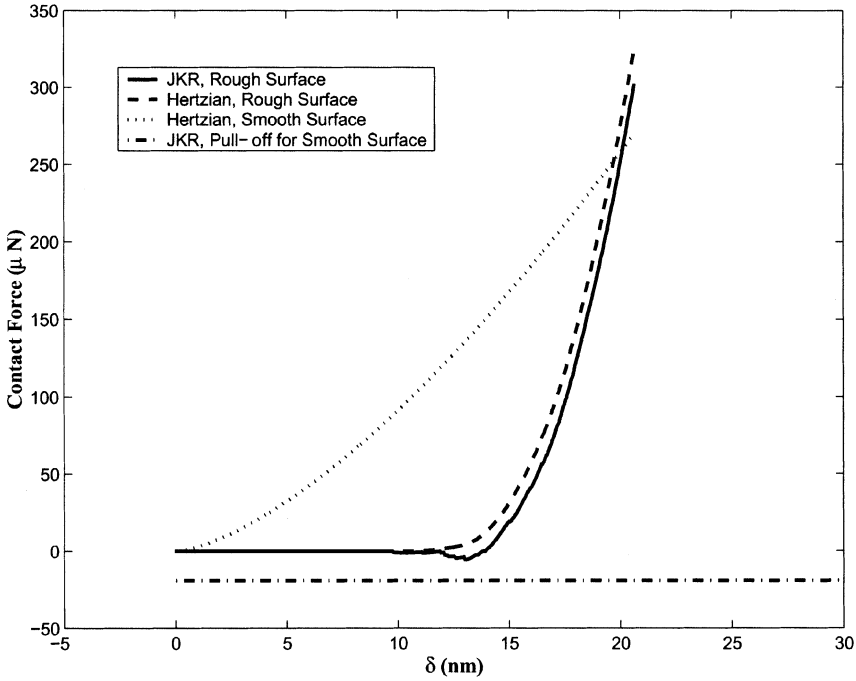

FIGURE 15 The load-displacement relationship for rough surface contact.

CONCLUSIONS

In this article, two simulation methods, the direct-simulation method and the asperity-superposition method, are introduced in order to simulate the contacts between a smooth sphere and a rough glass surface.

The simulation results show that the asperity peak detecting and least-squares surface-regression algorithm is accurate in representing the orientations, radii of curvature, and heights of the asperities obtained from surface AFM images. The difference between the original and reconstructed rough surface is negligibly small.

By comparison with the direct-simulation results, the asperity-superposition method is shown to be valid in modeling contact between a rough surface and a smooth sphere when the external load is small. The deformation of individual asperities is local and overlap between contact regions seldom occurs. When the load and the overall displacement are small, the methods of asperity superposition and direct simulation give similar contact force results. At the situation of

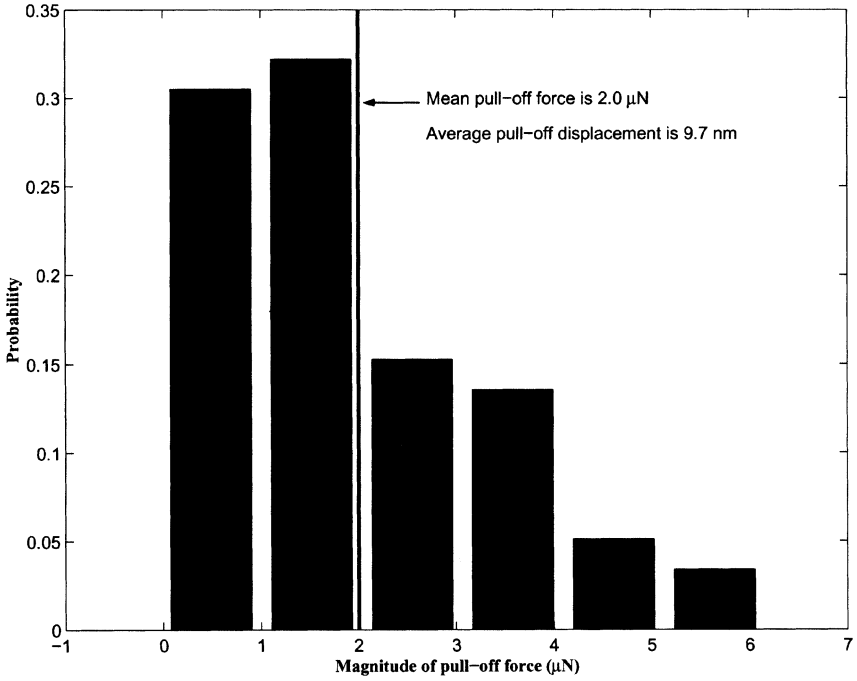

FIGURE 16 The mean load-displacement relationship for rough surface contact.

pull-off, both the external load and displacement are small and the contact regions do not overlap. Therefore, the superposition of asperity contacts based on the JKR model is valid in estimating the pull-off force for rough-surface contact. However, when the external load and displacement are high, the asperity-superposition model provides higher contact forces as compared with the direct-simulation model. To achieve a higher accuracy, the overlapping of contact regions and the elastic deformation of the rough surface must be modeled.

Simulations also show that the direct simulation model can solve the Hertzian contact problem accurately. The method is efficient in computing the surface displacement and contact pressure for rough-surface contact. An AFM image can be used directly without reconstruction. Modeling of individual asperity contacts is not needed. However, the method has difficulty in the simulation of contact with adhesion.

Elastic-contact simulations show that the contact force is related not only to the overall displacement but also to the locations of contact.

The contact force is distributed randomly over the rough surface and its probability density function changes with normal displacement. Adhesive contact results reveal that surface roughness reduces the sphere adhesion significantly. For the rough glass surface used in this study, the pull-off force was reduced by approximately 90% as compared with the smooth-surface contact case. Evidence that supports this result can be found in Kim *et al.* [11], Soltani [12] and the recent work of Ibrahim *et al.* [13].

These studies show that the contact with adhesion for surfaces with a roughness scale on the same order as the contact area is even more complicated because of surface complexity. A direct method of simulation considering the effects of free surface energy is needed. Experiments measuring the force of adhesion using an AFM also are needed to validate these simulation methods.

REFERENCES

[1] Greenwood, J. A., and Tripp, J. H., *Trans. ASME J. of Applied Mechanics*, **34**, 153–159 (1967).
[2] Greenwood, J. A., and Williamson, J. B. P., *Proc. Roy. Soc. Lond. A*, **295**, 300–319 (1966).
[3] Fuller, K. N. G., and Tabor, D., *Proc. R. Soc. London*, **345**, 327–342 (1975).
[4] Ogilvy, J. A., *J. Phys. D.: Appl. Phys.*, **25**, 1798–1809 (1992).
[5] Cheng, W., Dunn, P. F., and Brach, R. M., *J. Adhesion*, **78**, 1–37 (2002).
[6] Kalker, J. J., *Three-dimensional Elastic Bodies in Rolling Contact* (Kluwer Academic Publishers, Dordrecht, 2002).
[7] Jaeger, J., *Elastic Impact with Friction*, Ph.D. Dissertation, Technical University of Delft, Netherlands (2002).
[8] Abramowitz, M., and Stegun, I. A. (Eds.), *Handbook of Mathematical Functions with Formulas, Graphs, and Mathematical Tables* (Dover, New York, 1972), 9th Printing, Chap. 17, pp. 587–607.
[9] Johnson, K. L., *Contact Mechanics* (Cambridge University Press, Cambridge, 1985), pp. 76–77.
[10] Gilman, J. J., *J. Appl Phys.*, **31**(12), 2208–2217 (1960).
[11] Kim, H., Rockfold, L., and Russell, T., "Adhesion to Rough Surfaces" *American Physical Society 1999 Centennial Meeting Paper NPO1.156, March 20–26*, Atlanta, GA, USA, 1999.
[12] Soltani, M., *Mechanisms of Particle Removal Due to Turbulent Flow or Substrate Acceleration*, M.Sc. Thesis, Clarkson University Potsdam, NY (1993).
[13] Ibrahim, A. H., Dunn, P. F., and Brach, R. M., "Microparticle detachment from surfaces exposed to turbulent air flow: Controlled experiments and modeling," *J. Aerosol Sci*, **34**, 765–782 (2003).